Triosmium Clusters on a Support: Determination of Structure by X-ray Absorption Spectroscopy and High-Resolution Microscopy

ARTICLE *in* CHEMISTRY - A EUROPEAN JOURNAL · JANUARY 2011

Impact Factor: 5.73 · DOI: 10.1002/chem.201000860 · Source: PubMed

7 AUTHORS, INCLUDING:

Miaofang Chi
Oak Ridge National Laboratory
149 PUBLICATIONS **4,671** CITATIONS
SEE PROFILE

Bryan W. Reed
Integrated Dynamic Electron Solutions, Inc.
146 PUBLICATIONS **1,372** CITATIONS
SEE PROFILE

Norihiko L. Okamoto
Kyoto University
98 PUBLICATIONS **614** CITATIONS
SEE PROFILE

Bruce C Gates
University of California, Davis
597 PUBLICATIONS **14,602** CITATIONS
SEE PROFILE

CHEMISTRY
A EUROPEAN JOURNAL

DOI: 10.1002/chem.201000860

Triosmium Clusters on a Support: Determination of Structure by X-ray Absorption Spectroscopy and High-Resolution Microscopy

Shareghe Mehraeen,[a] Apoorva Kulkarni,[a] Miaofang Chi,[b] Bryan W. Reed,[c] Norihiko L. Okamoto,[a] Nigel D. Browning,*[a, c] and Bruce C. Gates*[a]

Abstract: The structures of small, robust metal clusters on a solid support were determined by a combination of spectroscopic and microscopic methods: extended X-ray absorption fine structure (EXAFS) spectroscopy, scanning transmission electron microscopy (STEM), and aberration-corrected STEM. The samples were synthesized from $[Os_3(CO)_{12}]$ on MgO powder to provide supported clusters intended to be triosmium. The results demonstrate that the supported clusters are robust in the absence of oxidants. Conventional high-angle annular dark-field (HAADF) STEM images demonstrate a high degree of uniformity of the clusters, with root-mean-square (rms) radii of 2.03 ± 0.06 Å. The EXAFS Os–Os coordination number of 2.1 ± 0.4 confirms the presence of triosmium clusters on average and correspondingly determines an average rms cluster radius of 2.02 ± 0.04 Å. The high-resolution STEM images show the individual Os atoms in the clusters, confirming the triangular structures of their frames and determining Os–Os distances of 2.80 ± 0.14 Å, matching the EXAFS value of 2.89 ± 0.06 Å. IR and EXAFS spectra demonstrate the presence of CO ligands on the clusters. This set of techniques is recommended as optimal for detailed and reliable structural characterization of supported clusters.

Keywords: aberration-corrected STEM · EXAFS spectroscopy · HAADF-STEM · MgO-supported clusters · osmium carbonyls

Introduction

Stabilized nanoparticles[1] exemplified by oxide-supported metal clusters,[2,3] have generated wide interest because they offer new and unique structures, reactivities, and catalytic properties that originate from their small sizes and interactions with the support; clusters with as few as three metal atoms have been reported.[4–7] Supported metal clusters and particles are important catalysts; the metals are typically Group 8 metals, and the supports are typically porous oxides or carbon. The support surfaces and the clusters themselves are almost always nonuniform in structure. The nonuniformity limits the structural information that can be obtained by methods such as spectroscopy or chemisorption of hydrogen or CO, and so determination of structure–reactivity relationships and the nature of the cluster–support interface has been challenging.

In attempts to overcome these limitations, researchers have worked to synthesize structurally uniform supported metal clusters.[2,8–15] One synthesis method involves the use of molecular metal clusters (such as metal carbonyls) as precursors, with the aim of retaining the metal frame in the supported clusters.[2,16–17]

Determination of the structures of the metal frames in supported metal clusters has benefited from recent advances in transmission electron microscopy (TEM); now, even the smallest metal clusters can be imaged.[16,18,19] The most informative images of metal clusters have been obtained with high-resolution scanning transmission electron microscopy (STEM).[6,20–24] Recent advances in STEM instruments and image analysis methods[25–27] have allowed determination of

[a] S. Mehraeen, A. Kulkarni, N. L. Okamoto, Prof. N. D. Browning, Prof. B. C. Gates
Department of Chemical Engineering and Materials Science
University of California, One Shields Avenue
Davis, California, 95616 (USA)
Fax: (+1) 530-752-1031
E-mail: nbrowning@ucdavis.edu
bcgates@ucdavis.edu

[b] Dr. M. Chi
Materials Science Division, Oak Ridge National Laboratory
Oak Ridge, Tennessee, 37830 (USA)

[c] Dr. B. W. Reed, Prof. N. D. Browning
Condensed Matter and Materials Division
Lawrence Livermore National Laboratory, Livermore
California 94550 (USA)

Supporting information for this article is available on the WWW under http://dx.doi.org/10.1002/chem.201000860.

structural details of the metal frames, and, as we show here, the highest-resolution STEM technique even allow resolution of individual metal atoms in appropriately synthesized supported metal clusters. The images come closest to determining the cluster structures when the clusters are smallest, containing only several metal atoms. However, the highest-resolution STEM techniques are limited by the sample damage caused by the high-intensity electron beam, which can fragment clusters, move them on supports, and cause metal aggregation. To minimize such damage, low-dose imaging techniques can be used, but then the images are often noisy and fail to provide the detailed structural information available from high-resolution STEM.

Our goal was to investigate the use of the high- and low-resolution STEM methods in concert with spectroscopy to determine how these methods provide the most information about cluster structures, and how the methods best complement each other. Because high-angle annular dark field (HAADF)-STEM images of supported clusters are optimized when the atoms in the clusters are heavy and those in the support are light, we chose clusters of a heavy transition metal (osmium) and a support with light atoms (MgO). To make clusters that are small and nearly uniform we used procedures described earlier[28–30] to make supported triosmium clusters by adsorption of $[Os_3(CO)_{12}]$, which has a triangular metal frame.[31,32] The support was chosen to be a porous high-area (approximately 70 m^2g^{-1}) MgO consisting of particles with a high degree of crystallinity; thus, the support itself lends itself to structural characterization by STEM.

Although the HAADF method in STEM is effective for characterization of local structures, it is unable to provide information about the ligands on the metal. Consequently, we also investigated the samples with extended X-ray absorption fine structure (EXAFS) and IR spectroscopies to identify the ligands on the clusters. EXAFS spectra also provide estimates of cluster sizes to complement STEM; the information provided by EXAFS spectroscopy is most exact when the clusters are smallest and most nearly uniform.

In an earlier investigation, EXAFS spectroscopy and STEM were used in concert to characterize samples similar to ours,[29] but the results were limited because of air exposure of the samples, leading to fragmentation of the clusters. Now, we have used air-exclusion techniques to avoid this complication, while also employing markedly improved microscopic methods.

Results

$[Os_3(CO)_{12}]$ has been used before as a precursor of oxide-supported metal clusters.[2,28,29,33,44,45] The structures of supported metal clusters synthesized from $[Os_3(CO)_{12}]$ have been characterized by IR,[28,29] Raman,[46] and EXAFS spectroscopies and TEM.[29] Various supports have been used for these samples, and often the cluster frame has evidently remained essentially intact. Thus, supported clusters formed from $[Os_3(CO)_{12}]$ are among the best-characterized supported metal clusters, and they have correspondingly been investigated in experiments to determine their reactivities and catalytic activities.

Our EXAFS and IR spectra confirm earlier results[29] and provide the opportunity to compare the spectroscopic results with images determined by STEM. Details follow.

Spectroscopic characterization of species formed by adsorption of $[Os_3(CO)_{12}]$ on MgO

IR spectra: The sample formed by room-temperature adsorption of $[Os_3(CO)_{12}]$ on partially dehydroxylated and decarbonated MgO that had been calcined at 673 K was bright yellow in color. The ν_{CO} region of the IR spectrum characterizing the adsorbed species includes bands at $\tilde{\nu}=$ 2075 (s), 2006 (vs), 1960 (w), and 1930 cm^{-1} (s) (Figure 1). The spectra indicate that carbonyl ligands were retained by the cluster after adsorption, and the band locations are consistent with reports[28,29] indicating the formation of $[Os_3(CO)_{11}]^{2-}$ on the MgO surface (referred to as $[Os_3(CO)_{11}]^{2-}$/MgO),[28] following from the work of Ugo et al.,[28] who interpreted their spectrum of an equivalently prepared samples on the basis of a comparison with that of authentic $[Os_3(CO)_{11}]^{2-}$ in solution and also that of the cluster anions that were extracted from the support into solution.[28] The evidence that the clusters are anionic implies that they are ion paired with the MgO surface.

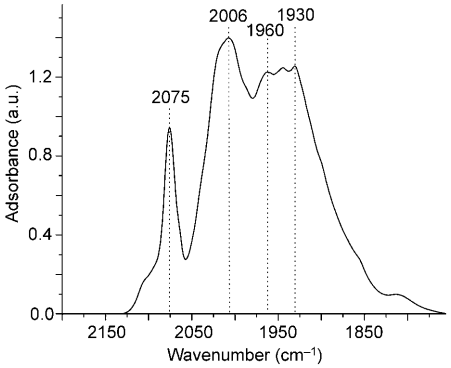

Figure 1. IR spectrum in the ν_{CO} region of species formed by adsorption of $[Os_3(CO)_{12}]$ on MgO that was calcined at 673 K.

EXAFS spectroscopy: Numerous models were considered in the analysis of the data characterizing the supported osmium carbonyls. The analysis resulted in three plausible models (Models I, II, and III, see Table 1) (the data could be fitted satisfactorily, in terms of goodness of fit, with any of the three). Model I includes Os–Os, Os–C, and Os–O* contributions (O* is a carbonyl oxygen). Model II includes Os–Os, Os–C, Os–$O_{support}$, and Os–O* contributions, and Model III includes Os–Os, Os–C, Os–Mg, and Os–O* contributions. Model II was selected because it provides the

Table 1. Fit diagnostic parameters for Models I, II, and III representing EXAFS data characterizing species formed by adsorption of $Os_3(CO)_{12}$ on MgO.[a]

Model	Δk [Å^{-1}]	ΔR [Å]	ε_v^2	Fit Variances Abs	Abs + Im
I	3.68–13.17	0.65–3.50	1.2	k^0: 0.09	k^0: 0.28
				k^1: 0.11	k^1: 0.38
				k^2: 0.21	k^2: 0.47
				k^3: 0.33	k^3: 0.70
II	3.68–13.17	0.65–3.50	3.5	k^0: 0.08	k^0: 0.26
				k^1: 0.13	k^1: 0.42
				k^2: 0.26	k^2: 0.68
				k^3: 0.43	k^3: 0.96
III	3.68–13.17	0.65–3.50	4.6	k^0: 0.19	k^0: 0.43
				k^1: 0.29	k^1: 0.84
				k^2: 0.64	k^2: 1.28
				k^3: 0.97	k^3: 1.56

[a] Model I includes Os–Os, Os–C, and Os–O* contributions; Model II includes Os–Os, Os–C, Os–$O_{support}$, and Os–O* contributions; Model III includes Os–Os, Os–C, Os–Mg, and Os–O* contributions; Abs, absolute part of the Fourier transformation; Im, imaginary part of the Fourier transformation; ε_v^2, goodness-of-fit parameter; k^n, weighting in the Fourier transformation.

best overall fit (see the Supporting Information). Although Model I is acceptable in terms of goodness of fit, it accounts for only Os–Os, Os–C, and Os–O* contributions—and therefore, not for the metal–support interface; besides failing to provide as good a fit as the other two models, it also fails to provide good fits of the individual shells. Thus, although the overall fit as shown by the overall goodness of fit values is satisfactory for Model I, we reject it because of the unsatisfactory fits of the individual shells. Model III also provides a good overall fit, but we also reject it in comparison with Model II, because the shell characterizing the Os–Mg contribution was found not to fit well after the contribution was phase- and amplitude-corrected, showing a too large value of ΔE_0 (-16 ± 6 eV) (this contribution is determined with low confidence). The Os–Os contribution, which is characterized by a coordination number of 2.5 ± 0.5, suggests the presence of triosmium clusters as does Model I (2.1 ± 0.4). Details are given in the Supporting Information.

Here, we discuss the details of the selected Model II (Table 2 and Figure 2). The Os–Os coordination number of 2.1 (Table 2) is consistent with the retention of the triangular osmium frame, as expected.[29] The Os–Os distance of 2.89 Å agrees with earlier results.[29] The Os–C and Os–O* contributions indicate carbonyl ligands on the cluster frame, characterized by multiple scattering, as expected. The Os–$O_{support}$ contribution at a distance of 2.16 Å, according to Table 2 is indicated clearly by the data, and the result is consistent with the literature[2] for clusters of Group 8 metals (even those saturated with CO ligands) on oxide and zeolite supports; the distance is a bonding distance.[2]

Table 2. Structural parameters corresponding to Model II for EXAFS data characterizing species formed by adsorption of $[Os_3(CO)_{12}]$ on MgO.[a]

Absorber–backscatterer pair	N	R [Å]	$10^3\times\Delta\sigma^2$ [Å^2]	ΔE_0 [eV]
Os–Os	2.1 ± 0.3	2.89 ± 0.01	5.2 ± 1.4	-3.9 ± 1.0
Os–C	3.2 ± 0.2	1.94 ± 0.01	8.3 ± 1.1	-0.5 ± 0.6
Os–O*	3.2 ± 0.2	3.03 ± 0.01	4.4 ± 6.4	-2.0 ± 0.2
Os–$O_{support}$	1.0 ± 0.1	2.16 ± 0.01	2.3 ± 2.2	4.0 ± 0.8

[a] The errors given in the table correspond to the precisions of the parameters. Notation: N = coordination number, R = interatomic distance, $\Delta\sigma^2$ = Debye–Waller parameter, ΔE_0, inner potential correction; the accuracies of the parameter are estimated to be as follows: N: ±20%, R: ±2% Å, $\Delta\sigma^2$: ±20%, ΔE_0: ±20%, but the accuracies may be less for the Os–$O_{support}$ contribution, which was not determined with as much confidence as the others.

The Os–$O_{support}$ interaction implies some distortion in the structure of the triosmium carbonyl (otherwise, the Os atoms would be shielded by the CO ligands and farther from the support surface). This implication is reinforced by the difference between the IR spectrum of the supported carbonylate anion and this anion in solution. We infer that distortion of the ligands was necessary to accommodate the clusters on the surface with maintenance of the charge balance and coordinative saturation of the clusters.

The EXAFS evidence of interactions between the Os atoms of the clusters and oxygen atoms of the MgO surface is consistent with this distortion and in general agreement with the literature of metal cluster carbonyl anions on oxide surfaces; specifically, the metal support–oxygen distance is in agreement with the literature generally for metal carbonyl cluster anions on oxide supports.[5]

The Os–$O_{support}$ distance is a typical bonding distance; the closeness of the Os atoms to support oxygen atoms implies that the Mg^{2+} ions that provide the charge for the carbonylate anions must be nearby on the surface, but the data are not sufficient to locate them in the nonuniform surface, and we cannot rule out the possibility of clusters anchored at or near defect sites, which might help alleviate some of the steric crowding. Because we lack the information to identify any defect sites where the clusters may be bonded, we caution that the EXAFS data indicating the average Os–$O_{support}$ coordination number of 1.0 ± 0.1 do not imply that all the clusters were flat, with each cluster Os atom interacting with one surface O atom; other orientations are possible.

Estimation by EXAFS spectroscopy of average size of triosmium carbonyl clusters supported on MgO: The average interatomic distances (R) determined in the analysis of the EXAFS data characterizing the supported clusters according to Model II for the Os–C, Os–O*, and Os–Os contributions were used to model the structure of the supported clusters. A triangular triosmium frame was assumed, consistent with the Os–Os coordination number (2.1) determined by EXAFS spectroscopy. We assumed that all the CO ligands were terminal, consistent with the IR spectra (Figure 3) (and with the structure of the precursor[31]). In view of the error in the Os–CO* coordination number (±20%), it was not possible to determine the number of CO ligands well. We approximate the value as about 11, because the IR spectrum of the supported species is similar to that of $[Os_3(CO)_{11}]^{2-}$, and this cluster has been reported to form on MgO upon adsorption of $[Os_3(CO)_{12}]$.[44] Thus, we propose

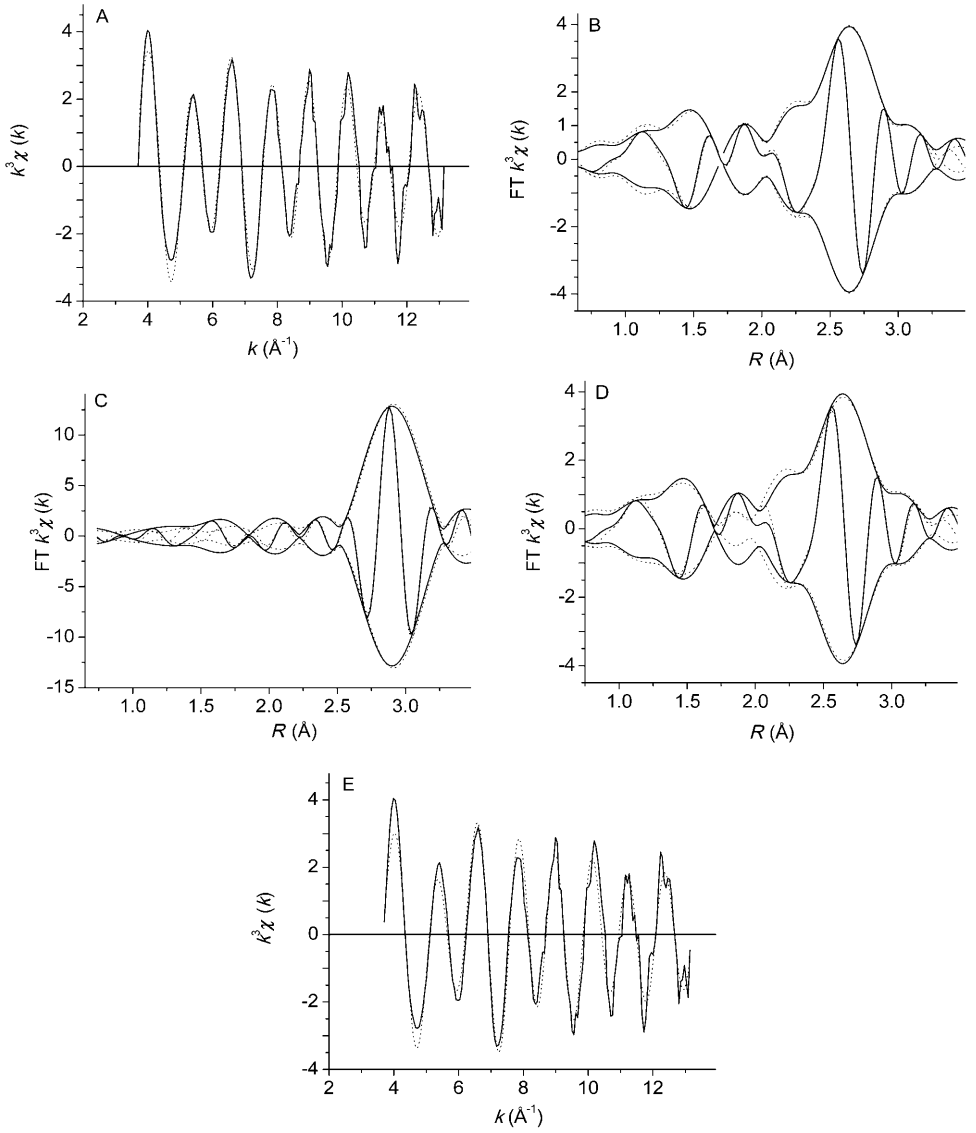

Figure 2. EXAFS data characterizing species formed by adsorption of $[Os_3(CO)_{12}]$ on MgO that was calcined at 673 K, for both Model I and Model II: A) k^3-weighted EXAFS function, $k^3(\chi)$ (solid line) and sum of the calculated contributions (dotted line) determined for Model II; B) k^3-weighted imaginary part and magnitude of the Fourier transform of the data (solid line) and sum of the calculated contributions (dotted line); C) k^3-weighted phase- and amplitude-corrected imaginary part and magnitude of the Fourier transform of the data (solid line) and calculated contributions (dotted line) of Os–Os shell; D) k^3-weighted imaginary part and magnitude of the Fourier transform of the data (solid line) and sum of the calculated contributions (dotted line) determined for Model I; E) k^3-weighted EXAFS function, $k^3(\chi)$ (solid line) and sum of the calculated contributions (dotted line) determined for Model I.

the structural model shown in Figure 3[1]. These simplifications were made because the orientations of the CO ligands in crystalline $[Os_3(CO)_{11}]^{2-}$ are close to this approximation.

This model was used to determine the average root-mean-square (rms) radius of the supported clusters (including the Os-C-O* distance), namely, 2.02 ± 0.04 Å. The details of the calculation are as stated elsewhere.[25,26] To be conservative in the estimate of the error in the rms radius, we used the upper error bound of the interatomic distances, namely, $\pm 2\%$[2]. We estimated the error in the rms radius by using a standard error propagation method,[29] finding a value of ± 0.04 Å. A schematic representation of the structure with these distances is shown in Figure 3.

Conventional HAADF-STEM characterization of triosmium carbonyl clusters supported on MgO: Figure 4A shows a

[1] For simplicity, for each Os atom assumed to be bonded to four CO ligands, two of the CO ligands were assumed to be oriented perpendicular to the triangular Os-Os-Os plane and the other two perpendicular to Os–Os edges. For the Os atom assumed to be bonded to three CO ligands, two of the CO ligands were assumed to be oriented perpendicular to the triangular Os-Os-Os plane and one perpendicular to Os–Os edges (consistent with crystal structure of $[Os_3(CO)_{11}]^{2-}$.

[2] Typically, the errors in the interatomic distance determined by EXAFS spectroscopy of samples such as ours are considered to be in the range of 1–2%.

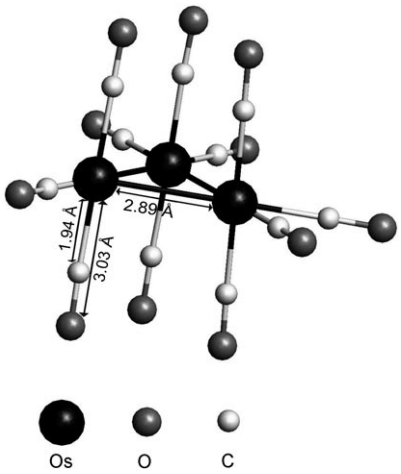

Figure 3. 3D model representing the structural parameters corresponding to Model II. The model is based on the EXAFS data (Table 2).

conventional STEM image of the sample synthesized by adsorption of $[Os_3(CO)_{12}]$ on MgO. Twenty seven clusters were analyzed to determine estimates of their total scattering probability (referred to as "mass", although the scaling with the physical mass is not quite linear) and the weighted rms radii. These values are presented in a scatter plot in Figure 4B. The data points appear to cluster into a few well-defined groups, with only a few ambiguous outlying points in each group. Likely interpretations of these groups arise naturally, given the structures and bond lengths determined from other methods,[31] the atomic scattering cross sections relevant to STEM, and the methods of analyzing upper and lower bounds for the orientation dependence of measured rms radii of anisotropic particles.[30]

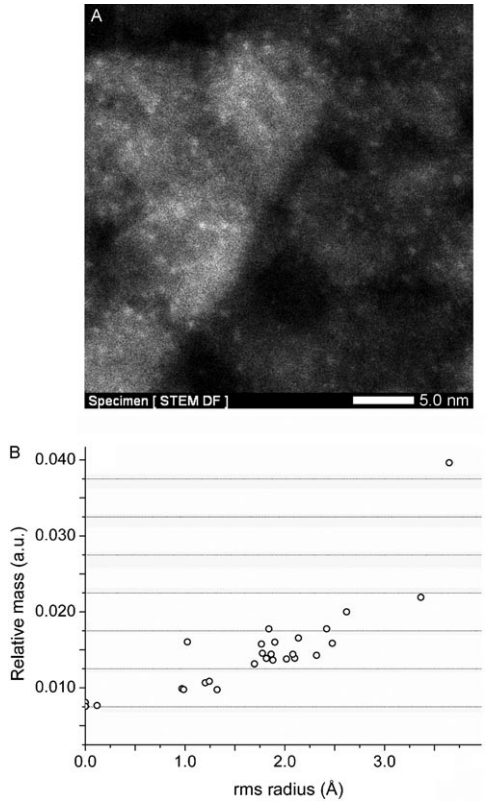

Figure 4. HAADF-STEM data characterizing species formed by adsorption of $[Os_3(CO)_{12}]$ on MgO that was calcined at 673 K. A) HAADF-STEM image. B) Correlation between mass and size in images of the species formed by adsorption of $[Os_3(CO)_{12}]$ on MgO.

The largest group of clusters, with a typical relative scattering probability (relative mass) of approximately 0.015 (normalized to the cluster with the highest intensity in the images) and a mean rms radius of 2.03 ± 0.06 Å, includes approximately 60% of the measured clusters (depending on the identity of the outliers)[3]. This group most likely represents largely intact $[Os_3(CO)_{11}]^{2-}$ clusters. The apparent rms radii of these clusters depend on orientation, ranging from approximately 1.85 to 2.34 Å (for the extreme cases of the electron beam being tangential to or normal to the Os_3 triangular plane) with a mean of 2.02 Å (assuming an isotropic orientation distribution). A few outlying clusters with radii greater than approximately 3 Å may consist of two or more triosmium carbonyl clusters in close proximity to each other, or they may be other species entirely. A second group, with a mean rms radius of 1.12 ± 0.06 Å and a mass roughly 2/3 that of the main group, may represent binuclear clusters. Assuming an Os–Os bond length of 2.88 Å, such clusters would appear in the STEM image to have rms radii ranging from approximately 1.0 to 2.0 Å, depending on the dumbbell orientation and the number and orientation of any retained CO groups. The third group, with an rms radius consistent with zero and a typical mass roughly half that of the main group probably consists of mononuclear osmium complexes with an undetermined number of CO ligands. Our data analysis method is unable to determine the sizes of clusters much smaller than the image resolution, such as those in which scattering arises from a single atom, and the method should produce an answer indistinguishable from zero in such cases.

In short, a majority of the clusters give profiles consistent with triosmium carbonyls, but a substantial fraction seem to have only one or two Os atoms. Furthermore, our analysis methods seem to be able to generate reliable population statistics and precise mean sizes within each subpopulation, even with fairly small sample sizes (thus, corroborating earlier applications and analyses of these methods).[26,27] We hypothesize that the smaller clusters were formed by fragmentation of triosmium carbonyls on the MgO surface, which was likely caused by electron beam damage.

Aberration-corrected high-resolution HAADF-STEM characterization of triosmium carbonyl clusters supported on MgO: The aberration-corrected high-resolution HAADF-STEM images demonstrate the presence of MgO with both long-range and short-range order crystallinity. Figure 5A displays typical aberration-corrected high-resolution HAADF-STEM images of the sample synthesized by ad-

[3] The intensities are not evident from visual examination of the images.

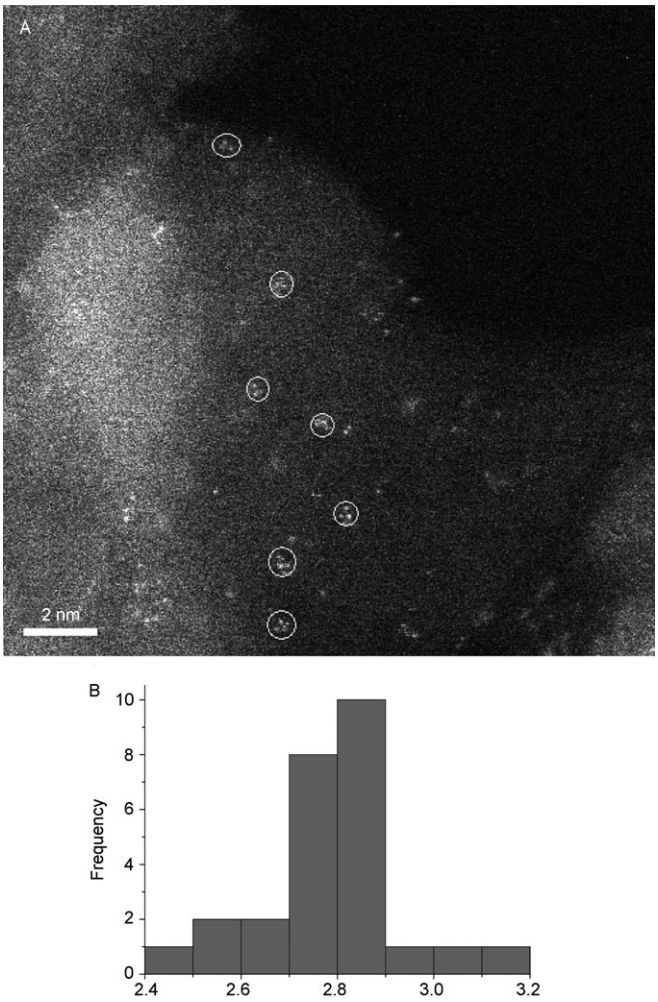

Figure 5. Aberration-corrected HAADF-STEM image characterizing species formed by adsorption of $[Os_3(CO)_{12}]$ on MgO that was calcined at 673 K. A) HAADF-STEM image. B) Histogram of *d* values for twenty six clusters.

sorption of $[Os_3(CO)_{12}]$ on MgO. The triosmium cluster frames are resolved atomically, and some examples are shown circled in the image. More images are presented in the Supporting Information. Although high-resolution STEM imaging reveals the clusters clearly, and the exposure of the imaged area to the electron beam was minimized, we cannot rule out the possibly of some beam damage—we suggest that beam damage was responsible for the presence of the fragmented clusters that were present with the intact triosmium clusters that are evident in the images.

Some regions of the images that were exposed to the beam for longer times clearly show effects of beam damage in aberration-corrected STEM (see the Supporting Information). This beam damage explains why we adopted the fast imaging and focusing methodology described in the Experimental Section.

The STEM images (Figure 5) show the 2D projections of 3D triosmium cluster frames. Twenty six 2D projections of triosmium frames were measured. As mentioned above, in the analysis we assumed that each triosmium frame is an equilateral triangle and calculated its side length *d* (i.e., the Os–Os distance) on the basis of its appearance in the projection. Figure 5B shows the histogram of the calculated *d* values for the twenty six clusters. The images yielded the average value of 2.80 ± 0.14 Å, with a narrow distribution.

In summary, the body of evidence lends support to two assertions: 1) many of the clusters probably were very nearly equilateral triangles before they were affected by the electron beam and 2) a simple data analysis method applied to the aberration-corrected STEM images is enough to determine a mean Os–Os bond length to a precision on the order of $\pm 5\%$, although the cluster orientations were not known a priori.

Comparison of rms radii of triosmium carbonyl clusters on MgO determined by EXAFS spectroscopy and conventional STEM and by XRD data characterizing crystalline $[Os_3(CO)_{11}]^{2-}$: For comparison with the rms radius of the supported triosmium carbonyl clusters calculated from the EXAFS data (2.02 ± 0.04 Å), we used XRD data[42] to calculate the rms radius of $[Os_3(CO)_{11}]^{2-}$ in the crystalline state (the method was similar to that described above for the supported clusters), finding a value of 2.02 ± 0.03 Å. Thus, these two values agree within error and reinforce our suggestion that the structure of the triosmium frame was retained after adsorption of $[Os_3(CO)_{12}]$ on MgO.

For a further comparison, the conventional STEM results shown in previous section indicate that the average rms radius of the intact clusters (those not affected by the electron beam) was 2.03 ± 0.06 Å. Thus, the cluster sizes determined by EXAFS spectroscopy and conventional STEM match within error, and the triosmium frame is essentially the same as that of the $[Os_3(CO)_{11}]^{2-}$ in the crystalline state.

Comparison of Os–Os distance in triosmium clusters on MgO determined by EXAFS spectroscopy and aberration-corrected high-resolution HAADF-STEM: The average Os–Os distance determined by EXAFS spectroscopy (Table 2) was found to be 2.89 ± 0.06 Å, and that determined by aberration-corrected HAADF-STEM was found to be 2.80 ± 0.14 Å (Figure 5B). Thus, these distances determined by the two techniques match each other within error.

Discussion

Previous reports of the characterization of supported triosmium carbonyl clusters[29] give evidence of the fragmentation of the clusters as a result of exposure to atmospheric O_2 and moisture. In contrast, we have found that the triosmium cluster frame was maintained intact when the samples were handled by rigorous air-exclusion techniques and with our sample transfer equipment, which evidently ensured sample integrity and allowed the quantitative comparison reported here.

The aberration-corrected STEM images provide evidence of the triosmium frames, with clear resolution of the Os

atoms; this is the first report of such resolution of the atoms in supported osmium clusters, and the images allow the calculation of interatomic distances between the Os atoms in the cluster frame. We regard this as a significant result for a class of supported metal cluster that is valuable for the reasons stated in the Introduction.

The evidence of intact cluster frames is clear, but the aberration-corrected STEM images also demonstrate that the samples were affected by beam damage. Beam damage is a major issue in imaging of samples such as ours by TEM and its importance is amplified in the aberration-corrected STEM because of the high electron dose. The effects of beam damage are expected to be fragmentation and/or aggregation of the clusters.[39] One reason why we used conventional STEM in concert with the aberration-corrected STEM was to evaluate the effects of the beam damage.

The images obtained by this lower-resolution microscopy (Figure 4A) confirm the presence of intact triosmium clusters and verify the major conclusion determined from the aberration-corrected STEM images by confirming the expectation that there was less beam damage in the conventional STEM imaging experiments. We emphasize that the interpretation of the STEM images required accounting for the fact that 2D images represent 3D clusters, and we calibrated the number of atoms by using the relative intensities to determine whether a particular bright spot in the image indicated a single Os atom or more than one. This type of image analysis led us to determine the exact nuclearities of the clusters.

Thus, the results presented here demonstrate the value of using these two TEM techniques in concert—the higher-resolution images provide essential detail of the metal cluster frames, and the lower-resolution images provide good estimates of the cluster size distributions, and the images from the two techniques together demonstrate the role of beam damage. The results point to the opportunity to use these two techniques to more fully elucidate the effects of beam damage in samples such as ours.

In summary, our data provide the most thorough microscopic evidence of supported clusters as small as triosmium, and they provide an excellent basis for comparing STEM results with EXAFS results for determination of cluster sizes and, specifically, for evaluating the uniformity of the clusters in the sample as a whole.

The information provided by the two STEM techniques is limited to the sizes of the metal frames and the distances between the Os atoms in the cluster frames. Determination of other structural information, such as identification of CO ligands, approximation of the number of CO ligands bonded to the cluster frames, and evidence of the interactions of the Os atoms in clusters with the MgO support requires complementary spectroscopic techniques: EXAFS spectroscopy provides the complementary information regarding the metal frame and the ligands bonded to it; IR spectroscopy provides further complementary information about the ligands.

Furthermore, the average Os–Os distance in the clusters was found by EXAFS spectroscopy to be 2.89 ± 0.06 Å (Table 2), which agrees within error with the Os–Os distance in the clusters determined from the aberration-corrected STEM images. This comparison confirms the high degree of uniformity of the sample indicated by the images (Figure 5). It is apparent from the results of the microscopy experiments that the fragments of the triosmium clusters result from electron beam damage that could not have affected the EXAFS data. The EXAFS results show that any such fragments that might have formed during the synthesis were such a small minority as to be undetectable within the error bounds of the EXAFS data. The literature of osmium carbonyl clusters on supports leads one to expect fragmentation in oxidative atmospheres (such as O_2[29]) but not under the conditions of our experiments.

This work demonstrates the power of combining multiple analysis techniques to obtain detailed information about the sizes, structures, and population statistics of supported clusters as small as triosmium. The results highlight the value of the high resolution attainable with aberration-corrected HAADF-STEM and the value of triosmium clusters for comparing the results of STEM and EXAFS data. We also emphasize the importance of applying rigorous sample-handling methods and complementary techniques to determine the structures of these supported clusters.

Conclusion

MgO-supported triosmium carbonyl clusters were prepared by adsorption of $[Os_3(CO)_{12}]$ on MgO and characterized by EXAFS and IR spectroscopies and conventional and aberration-corrected high-resolution HAADF-STEM. Conventional STEM and EXAFS spectroscopy indicated the rms radii of supported triosmium carbonyl clusters to be 2.03 ± 0.06 and 2.02 ± 0.04 Å, respectively. Aberration-corrected STEM and EXAFS spectroscopy determined the Os–Os distances in the triosmium clusters to be 2.80 ± 0.14 and 2.89 ± 0.06 Å, respectively. These comparisons show a satisfying agreement among the methods at a high level of accuracy, thus, yielding much greater confidence in the results than could be provided by any one technique alone. This work demonstrates details of the sizes and structures of supported triosmium clusters for the first time by taking advantage of the complementarity of aberration-corrected STEM, conventional STEM, and EXAFS spectroscopy.

Experimental Section

Sample preparation and handling

Methods and materials: Supported triosmium clusters were synthesized on the surface of MgO powder from $[Os_3(CO)_{12}]$.[28,29] Synthesis and handling were performed with exclusion of air and moisture on a double-manifold Schlenk line and in an N_2-filled glovebox (AMO-2032, Vacuum Atmospheres). *n*-Pentane solvent (Aldrich) was refluxed under N_2 in the presence of sodium/benzophenone ketyl to remove traces of water and

then deoxygenated by sparging of dry N_2 prior to use. $[Os_3(CO)_{12}]$ (Strem, 99%) was used as received. The MgO powder (EM Science, 70 m^2g^{-1}) was pretreated by calcination in flowing O_2 (Airgas, 99.999%) at 673 K for 6 h and evacuation at 673 K for 14 h.

Synthesis of supported triosmium carbonyl clusters: The MgO-supported samples were prepared, as before,[29] by slurrying $[Os_3(CO)_{12}]$ with the calcined MgO powder in *n*-pentane under N_2 for 24 h at room temperature followed by overnight evacuation at 298 K to remove the solvent. A calculated amount of $[Os_3(CO)_{12}]$ was added to the MgO support to give samples containing 1.0 wt% Os when all the added osmium remained on the support,[33] and the synthesis method assured that it did.

Characterization methods

IR spectroscopy: Transmission spectra were recorded with a Bruker IFS-66v/s spectrometer with a spectral resolution of 2 cm^{-1}. Samples were pressed into self-supporting wafers and mounted in the cell (International Crystal Laboratories) and sealed in the N_2-filled glovebox.

EXAFS spectroscopy: EXAFS experiments were performed at X-ray beam line X-18B at the National Synchrotron Light Source at Brookhaven National Laboratory. The storage ring operated with an electron energy of 3 GeV; the ring current was in the range 60–100 mA. Both the supported osmium carbonyl clusters and the decarbonylated clusters were characterized by EXAFS spectroscopy. In an argon-filled glovebox at the synchrotron, each powder sample was pressed into a self-supporting wafer. The sample mass was chosen to give an X-ray absorbance of 2.5 at the $Os_{L_{III}}$ edge (10871 eV). The wafer was loaded into an EXAFS cell,[34] sealed under a positive N_2 pressure, and removed from the glovebox. The cell was then evacuated (10^{-5} mbar), and the sample was aligned in the X-ray beam and cooled to nearly liquid-nitrogen temperature. EXAFS spectra were then collected in transmission mode. Higher harmonics in the X-ray beam were minimized by detuning the Si (111) monochromator by 20–25% at the $Os_{L_{III}}$ edge. The reported spectrum is the average of four.

Conventional HAADF-STEM: Images of the samples were acquired by the HAADF method in STEM mode with a 200 kV JEOL JEM-2500SE TEM/STEM instrument, with a probe size of 0.3 nm at full-width half-maximum, a convergence semi-angle of 12 mrad, and a collection semi-angle in the range of 35–90 mrad. To protect the air-sensitive samples from exposure to the atmosphere, they were handled in an N_2-filled glovebox with O_2 and moisture concentrations less than 1 ppm. A 200 mesh copper grid with a holey carbon film was dipped into the sample powder in the glovebox. The grids were then loaded onto a Fischione vacuum-transfer-holder (Model 2020) and transferred to the microscope without exposure of the samples to air. Further details of the sample holder and the transfer method are given elsewhere.[25]

Aberration-corrected high-resolution HAADF-STEM: The samples in stainless-steel tubes that are commonly used for handling samples for ultrahigh-vacuum experiments (sealed with O-rings) were transported to Oak Ridge National Laboratory (ORNL) for microscopy experiments. At ORNL, the samples were handled in an argon-filled glovebag. The glovebag was purged 20 times with argon before use. The tubes containing the sample were opened in the glovebag, and the samples were placed onto copper grids (200 mesh). The sample holder was transferred from the glovebag to the microscope with an air exposure of at most approximately 2 s.

The method of sample preparation was the same as that used in the conventional HAADF-STEM imaging experiments described in the previous section.[25,26] High-resolution HAADF-STEM images of the sample were acquired with an aberration-corrected JEOL 2200 FS microscope, with the convergence angle being 26.5 mrad and the collection inner angle 100 mrad. Imaging of nanoclusters as small as ours by TEM is challenging because of possible effects of the electron beam on the sample. To minimize the artifacts in the images caused by beam damage, the microscope was aligned for one region of the sample, and then the beam was shifted to a neighboring region for a quick image acquisition: 4 s for a 512×512 pixel size. This methodology ensured that the exposure of the imaged area to the electron beam was minimal.

EXAFS data analysis: The X-ray absorption-edge energy was calibrated with the measured signal of a hafnium foil (scanned simultaneously with the sample) at the $Hf_{L_{II}}$ edge. The $Hf_{L_{II}}$ edge (10739 eV) was chosen because of its proximity to the $Os_{L_{III}}$ edge (10871 eV). Data reduction and analysis were carried out with the average of the four scans, by use of the software XDAP.[35] XDAP was used for edge calibration, deglitching, data normalization, and conversion of the data into an EXAFS (chi) file.[36] The software FEFF7[37] was used to determine amplitude- and phase-shift functions by theoretical calculations for reference materials with known crystal structures, except that experimental EXAFS results were used as a reference for Os–C and Os–O* contributions. The reference compounds used for each EXAFS contribution are summarized in the Supporting Information. Analysis was carried out with unfiltered data; the Fourier-transformed $\chi(k)$ data were fitted in R space (R is distance from the absorbing Os atom, χ is the EXAFS function).[36] The objective function used for the least-squares data fitting is reported elsewhere.[35] Both the magnitude and the imaginary part of the Fourier-transformed data were fitted with k^0, k^1, k^2, and k^3 weightings of the data until the fit was optimized.

XDAP allowed the efficient application of a difference-file technique[36] for determination of optimized fit parameters. The postulated models used in the data fitting included Os–Os, Os–C, Os–O*, Os–Mg, and Os–$O_{support}$ contributions. The Os–C and Os–O* contributions in each model are characterized by multiple scattering (as expected for linear Os-C-O* moieties), as was evident in the fitting; to distinguish such contributions from single-scattering contributions, phase and amplitude correction was used.

The EXAFS data were analyzed with a maximum of sixteen free parameters over the ranges $3.68 \le k \le 13.17$ Å^{-1} and $0.65 \le R \le 3.50$ Å. The number of parameters used in the fitting was always less than the statistically justified number, calculated with the Nyquist theorem,[36] $n = (2\Delta k\Delta R/\pi)+2$, where Δk and ΔR, respectively, are the k and R ranges used in the fitting. To estimate the statistical error associated with the $\chi(k)$ values for each data set (used in the estimation of precisions), the averaged data were Fourier filtered by using a k window larger than that used for the fitting. The filtered data were then subtracted from the raw data to obtain an estimate of the error at each point. The root-mean-square error was calculated and used for the calculation of precisions and the goodness of fit. The approximate accuracies of the fit parameters characterizing the absorber–backscatterer pair contributions are estimated to be as follows: coordination number N: ±20%, distance R: ±2% Å, Debye–Waller factor $\Delta\sigma^2$: ±20%, and inner potential correction ΔE_0: ±20%. The precisions reported for each of the parameters in the EXAFS models were calculated on the basis of the objective function of the fitting routine.[36] The values of the goodness of fit (recommended by the International XAFS Society[38]) are included with each fit.

Numerous models were considered in the analysis of EXAFS data. The analysis resulted in three plausible fit models (Model I, Model II, and Model III)—by this, we mean that each data set could be fitted satisfactorily (in terms of goodness of fit) with all three models. Model II was chosen as the one best representative of the structure of the supported species. The values of the structural parameters determined with each of the models and the reasoning underlying the model selection are given in the Supporting Information.

STEM data analysis

Conventional HAADF-STEM: In the microscopy experiments the accuracy in the size determination of the supported clusters is limited by the size of the electron probe and the instability of the clusters under the influence of the electron beam (beam damage).[39] Reduction of the electron dose can minimize the effects of the beam, but at the expense of signal-to-noise ratio. We used a relatively low electron dose to achieve the benefit of sample stability, and, to compensate for the resultant noise in the images, we used a blurring propagation method of image analysis; details are given elsewhere.[26] The analysis method produces an estimate of the population distribution of root-mean-square (rms) particle radii, with each atom weighted according to its electron scattering cross section (a function of the electron kinetic energy and angular detection range), and a total "mass" (the total scattering probability) for each particle.

Aberration-corrected high-resolution HAADF-STEM: The sample was also imaged by aberration-corrected STEM to yield atomic-resolution images of the triosmium clusters. Individual Os atoms are distinctly visible in the images, allowing direct interpretation of the triangular cluster geometry apart from the fact that the orientation of the triosmium plane relative to the electron beam direction is unknown. Thus, we can directly measure pairwise interatomic distances a, b, and c as projected onto the imaging plane, but the degree of foreshortening must be inferred. Previous work[31,32,40–43] on triosmium carbonyl anions and neutral triosmium carbonyl clusters in the crystalline state indicates that the triosmium frames are very nearly equilateral triangles; examples are listed in the Supporting Information. Thus, we hypothesize that each triosmium cluster is, to a good approximation, an equilateral triangle of side length d. We determine d according to Equation (1)

$$d = \frac{\sqrt{a^2 + b^2 + c^2 + \sqrt{2}\sqrt{(a^2 - b^2)^2 + (b^2 - c^2)^2 + (a^2 - c^2)^2}}}{\sqrt{3}} \quad (1)$$

which is derived in the Supporting Information on the basis of analytic geometry. We then compared this value of d with those determined from the EXAFS and conventional STEM measurements. When the values match (within error), then we claim that the structure observed in the aberration-corrected STEM is consistent with the hypothesis of an equilateral triangle. Otherwise, we conclude that some other structure is present (modified perhaps as a result of interactions with the support or of breaking of bonds in the cluster by the high-energy electrons). Without tomographic techniques (which are very difficult for radiation-sensitive materials), it is impossible to be sure that any given frame is truly equilateral. However, if most such frames consistently yield the expected d values, we can confidently infer that many of the frames are nearly equilateral triangles.

Acknowledgements

This work was supported by the National Science Foundation, GOALI Grant CTS-05-00511. We acknowledge the National Synchrotron Light Source, a national user facility operated by Brookhaven National Laboratory on behalf of the US Department of Energy, Office of Science, Basic Energy Sciences, for access to beam time at beam line X-18B. The electron microscopy experiments were performed at the Oak Ridge National Laboratory SHaRE User Facility, which is supported by the Division of Scientific User Facilities, DOE Office of Science, Basic Energy Sciences. We thank ExxonMobil for partial support of this work.

[1] J.-M. Ha, A. Solovyov, A. Katz, *Langmuir* **2009**, *25*, 10548.
[2] J. C. Fierro-Gonzalez, S. Kuba, Y. Hao, B. C. Gates, *J. Phys. Chem. B* **2006**, *110*, 13326.
[3] N. de Silva, A. Solovyov, A. Katz, *Dalton Trans.* **2010**, *39*, 2194.
[4] A. M. Argo, J. F. Goellner, B. L. Phillips, G. A. Panjabi, B. C. Gates, *J. Am. Chem. Soc.* **2001**, *123*, 2275.
[5] J. Guzman, B. C. Gates, *J. Am. Chem. Soc.* **2004**, *126*, 2672.
[6] S. I. Sanchez, L. D. Menard, A. Bram, J. H. Kang, M. W. Small, R. G. Nuzzo, A. I. Frenkel, *J. Am. Chem. Soc.* **2009**, *131*, 7040.
[7] J. H. Kang, L. D. Menard, R. G. Nuzzo, A. I. Frenkel, *J. Am. Chem. Soc.* **2006**, *128*, 12068.
[8] J. E. Mondloch, X. Yan, R. G. Finke, *J. Am. Chem. Soc.* **2009**, *131*, 6389.
[9] M. J. Manard, P. R. Kemper, M. T. Bowers, *J. Am. Chem. Soc.* **2005**, *127*, 9994.
[10] A. Uzun, B. C. Gates, *J. Am. Chem. Soc.* **2009**, *131*, 15887.
[11] X. Tong, L. Benz, P. Kemper, H. Metiu, M. T. Bowers, S. K. Buratto, *J. Am. Chem. Soc.* **2005**, *127*, 13516.
[12] A. Kulkarni, B. C. Gates, *Angew. Chem.* **2009**, *121*, 9877; *Angew. Chem. Int. Ed.* **2009**, *48*, 9697.
[13] S. Chrétien, S. K. Buratto, H. Metiu, *Curr. Opin. Solid State Mater. Sci.* **2007**, *11*, 62.
[14] S. Vajda, M. J. Pellin, J. P. Greeley, C. L. Marshall, L. A. Curtiss, G. A. Ballentine, J. W. Elam, S. Catillon-Mucherie, P. C. Redfern, F. Mehmood, P. Zapol, *Nat. Mater.* **2009**, *8*, 213.
[15] S. Lee, L. M. Molina, M. J. López, A. J. Alonso, B. Hammer, B. Lee, S. Seifert, R. E. Winans, J. W. Elam, M. J. Pellin, S. Vajda, *Angew. Chem.* **2009**, *121*, 1495; *Angew. Chem. Int. Ed.* **2009**, *48*, 1467.
[16] M. S. Nashner, A. I. Frenkel, D. L. Adler, J. R. Shapley, R. G. Nuzzo, *J. Am. Chem. Soc.* **1997**, *119*, 7760.
[17] A. M. Argo, J. F. Odzak, B. C. Gates, *J. Am. Chem. Soc.* **2003**, *125*, 7107.
[18] L. D. Menard, H. Xu, S. P. Gao, R. D. Twesten, A. S. Harper, Y. Song, G. Wang, A. D. Douglas, J. C. Yang, A. I. Frenkel, R. W. Murray, R. G. Nuzzo, *J. Phys. Chem. B* **2006**, *110*, 14564.
[19] L. F. Allard, G. A. Panjabi, S. N. Salvi, B. C. Gates, *Nano Lett.* **2002**, *2*, 381.
[20] S. I. Sanchez, M. W. Small, J. M. Zuo, R. G. Nuzzo, *J. Am. Chem. Soc.* **2009**, *131*, 8683.
[21] S. J. Pennycook, D. E. Jesson, A. J. McGibbon, P. D. Nellist, *J. Electron Microsc.* **1996**, *45*, 36.
[22] J. Sun, M. Chi, R. J. Lobo-Lapidus, S. Mehraeen, N. D. Browning, B. C. Gates, *Langmuir* **2009**, *25*, 10754.
[23] V. A. Bhirud, M. J. Moses, D. A. Blom, L. F. Allard, T. Aoki, S. Mishina, C. K. Narula, B. C. Gates, *Microsc. Microanal.* **2005**, *11*, 1574.
[24] A. Uzun, V. Ortalan, Y. Hao, N. D. Browning, B. C. Gates, *ACS Nano* **2009**, *3*, 3691.
[25] A. Kulkarni, S. Mehraeen, B. W. Reed, N. L. Okamoto, N. D. Browning, B. C. Gates, *J. Phys. Chem. C* **2009**, *113*, 13377.
[26] N. L. Okamoto, B. W. Reed, S. Mehraeen, A. Kulkarni, D. G. Morgan, B. C. Gates, N. D. Browning, *J. Phys. Chem. C* **2008**, *112*, 1759.
[27] B. W. Reed, D. G. Morgan, N. L. Okamoto, A. Kulkarni, B. C. Gates, N. D. Browning, *Ultramicroscopy* **2009**, *110*, 48.
[28] R. Psaro, C. Dossi, R. Ugo, *J. Mol. Catal.* **1983**, *21*, 331.
[29] V. A. Bhirud, H. Iddir, N. D. Browning, B. C. Gates, *J. Phys. Chem. B* **2005**, *109*, 12738.
[30] F. B. M. Duivenvoorden, D. C. Koningsberger, Y. S. Uh, B. C. Gates, *J. Am. Chem. Soc.* **1986**, *108*, 6254.
[31] E. R. Corey, L. F. Dahl, *Inorg. Chem.* **1962**, *1*, 521.
[32] M. R. Churchill, B. G. DeBoer, *Inorg. Chem.* **1977**, *16*, 878.
[33] H. H. Lamb, A. S. Fung, P. A. Tooley, J. Puga, T. R. Krause, M. J. Kelley, B. C. Gates, *J. Am. Chem. Soc.* **1989**, *111*, 8367.
[34] R. E. Jentoft, S. E. Deutsch, B. C. Gates, *Rev. Sci. Instrum.* **1996**, *67*, 2111.
[35] M. Vaarkamp, J. C. Linders, D. C. Koningsberger, *Phys B Conden. Matt.* **1995**, *208–209*, 159.
[36] D. C. Koningsberger, B. L. Mojet, G. E. Van Dorssen, D. E. Ramaker, *Top. Catal.* **2000**, *10*, 143.
[37] A. L. Ankudinov, J. J. Rehr, *Phys. Rev. B* **1997**, *56*, R1712.
[38] In International XAFS Society, Error Reporting Recommendations: A Report of the Standards and Criteria Committee. http://fisica.unicam.it/IXS/OLD/subcommittee_reports/sc/err-rep.pdf, **2006**.
[39] P. E. Batson, N. Dellby, O. L. Krivanek, *Nature* **2002**, *418*, 617.
[40] J. A. Krause, U. Siriwardane, T. A. Salupo, J. R. Wermer, D. W. Knoeppel, S. G. Shore, *J. Organomet. Chem.* **1993**, *454*, 263.
[41] H.-G. Ang, S.-G. Ang, W.-L. Kwik, Q. Zhang, *J. Organomet. Chem.* **1995**, *485*, C10.
[42] B. F. G. Johnson, J. L. Ebbe Nordlander, P. R. Raithby, *J. Chem. Soc. Dalton Trans.* **1996**, 3825.
[43] K. Biradha, V. M. Hansen, W. K. Leong, R. K. Pomeroy, M. J. Zaworotko, *J. Cluster Sci.* **2000**, *11*, 285.
[44] H. H. Lamb, B. C. Gates, *J. Phys. Chem.* **1992**, *96*, 1099.
[45] E. Cariati, D. Roberto, R. Ugo, E. Lucenti, *Chem. Rev.* **2003**, *103*, 3707.
[46] M. Deeba, B. J. Streusand, G. L. Schrader, B. C. Gates, *J. Catal.* **1981**, *69*, 218.

Received: April 6, 2010
Published online: November 23, 2010

